



Cite this: *CrystEngComm*, 2021, 23, 8379

Received 3rd September 2021,
Accepted 2nd November 2021

DOI: 10.1039/d1ce01199e

rsc.li/crystengcomm

Nucleation behaviour of racemic and enantiopure histidine†

Lina C. Harfouche,^a Simon Clevers,^a Gérard Coquerel^a and Ivo B. Rietveld^{id}*^{ab}

Nucleation of D,L- and L-histidine is examined using induction time measurements and their nucleation rates have been deduced. Results indicate a much slower nucleation for the racemic form compared to the pure enantiomer form. The effect of temperature and supersaturation on the nucleation rate is also described. Classical nucleation theory (CNT) is used to determine the interfacial energy, the nucleation energy barrier, and the nucleus size for both compounds. The large difference between the nucleation rates for the pure enantiomer and the racemic compound have so far not led to satisfactory preferential crystallization; however second harmonic generation analysis demonstrates the presence of non-centrosymmetric domains embedded within the racemic crystals implying that improving control over the nucleation conditions may lead to more efficient preferential crystallisation and symmetry breaking.

Introduction

Crystallization is an important industrial process; it is commonly used in several important industries including pharmaceuticals,¹ chemicals,² food,³ pigments,⁴ and microelectronics,⁵ in which crystallization is often used as a final separation and purification step to control the crystal size, shape, composition, and structure.⁶ Crystallization is used to manipulate the end-product's physical and chemical properties (polymorph, solubility, morphology, density, size, size distribution, *etc.*)⁷ especially in the pharmaceutical industry, because many pharmaceutical ingredients are manufactured in a solid, crystalline form. Ultimate control over the crystallization process requires a control of the most crucial step: 'nucleation'.

Nucleation can happen through different mechanisms that can be divided into two categories:^{6–8} primary nucleation and secondary nucleation. The critical nucleus may emerge either homogeneously or heterogeneously on a foreign surface such as dust particles or the wall of the container.^{9,10} Heterogeneous nucleation is often faster and more common than homogeneous nucleation because a surface is always present in the reaction environment.¹¹ However, nucleation is difficult to control because several factors (*e.g.* nucleation rate, the number of molecules needed to form a nucleus of a

critical size, the energy barrier, *etc.*)⁶ can play a major role in the nucleation onset.

In this study, racemic and enantiopure histidine (Scheme 1) have been selected as model compounds, as control over nucleation is one of the pathways to accomplish chiral resolution through crystallisation. We aim to compare the nucleation behaviour of the racemic and enantiopure materials. To the best of our knowledge, this kind of studies are rare.¹²

We will apply a previously developed method based on induction time measurements^{13,14} to determine the nucleation kinetics of the model compounds. The experimental data will be analysed against classical nucleation theory^{15,16} based on Arrhenius rate laws. In addition, the effect of temperature and supersaturation is studied.

Materials and methods

Materials

Racemic (D,L) and enantiopure (L)-histidine (purity ≥ 99.0%) were purchased from Merck and used as received. Water used in this work is demineralized water.



Scheme 1 Chemical structure of D-histidine. The chiral centre is denoted with an asterisk.

^a Université de Rouen Normandie, UFR des Sciences et Techniques, Laboratoire SMS-EA3233, Place Emile Blondel, 76821, Mont-Saint-Aignan, France.

E-mail: ivo.rietveld@univ-rouen.fr

^b Université de Paris, Faculté de Pharmacie, 4 avenue de l'observatoire, 75006, Paris, France

† Electronic supplementary information (ESI) available. See DOI: 10.1039/d1ce01199e



SHG microscopy. Insight X3 single laser with automated dispersion compensation (Spectra-Physics, Santa Clara, USA) and a TCS SP8 MP confocal microscope (Leica Microsystems, Wetzlar, Germany) performed confocal microscopy as well as two-photon microscopy and fluorescence lifetime imaging of the samples. The laser cavity had over 2.44 W of average power at 900 nm and was tunable from 680 nm to 1300 nm. The repetition rate was 80 MHz and the temporal width at the output of the cavity was around 120 fs (<100 fs between 850 nm and 1050 nm). The laser was controlled with the LASX Leica software. Two Leica hybrid descanned detectors (HyD) were used to record images. For two-photon imaging experiments, fluorescence was collected after the microscope objective *via* a dichroic beam splitter, transparent to wavelengths greater than 815 nm. Microscope objectives were long working distance dry Leica objectives (HC PL Fluotar 5 \times NA 0.15, HC PL Fluotar 10 \times NA 0.3 or HC PL APO 20 \times NA 0.4

According to Kurtz and Perry SHG powder method,¹⁹ SHG signal intensities were compared to the signal of a reference compound (α -quartz powder – 45 μm average size).

Classical nucleation theory. As nucleation is regarded as a random process, the nucleation rate can be obtained with a cumulative probability distribution of the induction time (t_i) as reported elsewhere.¹⁴ The cumulative probability $P(t)$ to detect crystals at a time t is given by:

Experimentally, the cumulative probability function, $P(t)$, is defined as follows:

Nucleation kinetic parameters

The temperature dependence of the nucleation rate can be modelled with an Arrhenius-type equation. The natural logarithm of J/β is a linear function of $\ln^{-2}\beta$ as shown in eqn (3); the data have been accordingly plotted in Fig. 2. The resulting slopes and intercepts are used to determine the experimental thermodynamic parameter B_{exp} and kinetic parameter A_{exp} respectively. The considered model does not afford an understanding of the origins of the experimentally observed not perfect linear plots and variations for L-histidine at different temperature as seen in Fig. 2. Polymorphism of L-histidine (LHISTD01, LHISTD10) might be a reason for the relatively scattered data, however, XRD measurements of the final powders did not provide any proof that a second polymorph was present.²⁶

The prediction of the kinetic parameter for homogeneous interface-transfer control $A_{I,\text{hom(predicted)}}$ is obtained from eqn (7). The thermodynamic parameter $B_{\text{hom(predicted)}}$ is obtained theoretically by substituting $\gamma_{\text{predicted}}$ in eqn (4). The results are very similar to the one obtained by substituting a_1 and b_1 in eqn (9).

Experimental values of the interfacial energy (γ_{exp}) have been obtained from the B_{exp} values using eqn (4). The theoretical values of the interfacial energies ($\gamma_{\text{predicted}}$) have been calculated using eqn (8).

All results for L and DL-histidine are presented and compared in Table 2.

Only the results for interface-transfer control are shown here, those for volume-diffusion control obtained by linearizing the equation of J for volume-diffusion control

The experimental cumulative probability distributions $P(t)$ as a function of the measured induction times t_i in seconds are given in Fig. S3 and S4 in the ESI.†

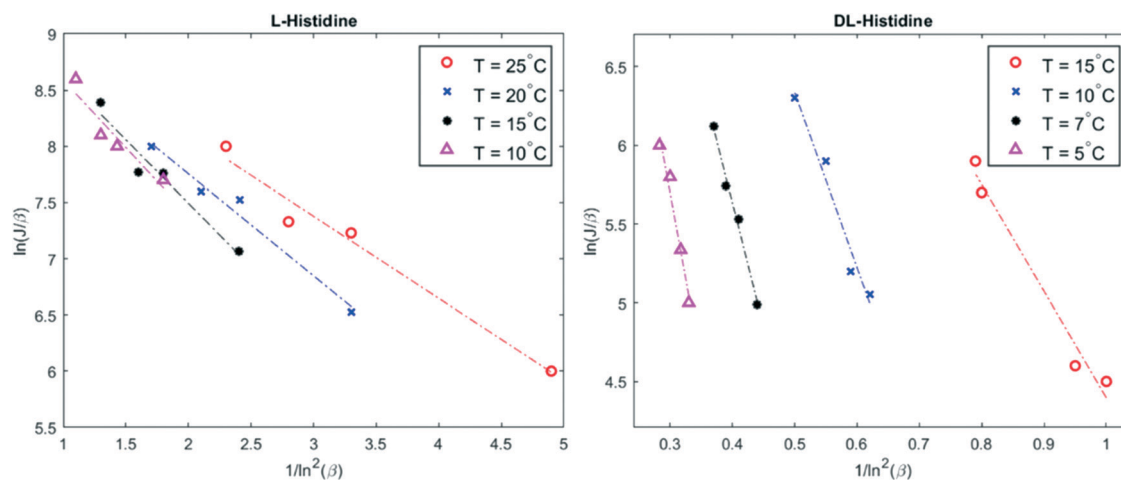


Fig. 2 Plot of $\ln(J/\beta)$ versus $1/\ln^2\beta$ for four different temperatures. The experimental data are given by colored marker shapes and the dotted lines are the best fit to the experimental points.

CrystEngComm, 2021, 23, 8379–8385 | 8383



Fig. 3 Overlay of SHG and microscope image demonstrating small non-centrosymmetric domains in the racemic crystal.

composition is tolerated by the 'racemic' crystal lattice. Considering the foregoing nucleation analysis, it is possible that in the highly supersaturated racemic system, initial nucleation of enantiomerically enriched crystals occurs. However, subsequently, crystal growth is taken over by the more stable and less soluble racemic crystal. These observations are consistent with a report on limited preferential enrichment observed for histidine³¹ and would explain the weak SHG effect in line with symmetry breaking through crystallisation.^{32,33} It also explains, in the case of the racemic compound, why CNT may not work as the nucleation is clearly not a simply homogeneous process.

Conclusions

Nucleation induction time in water has been determined for two systems: racemic histidine and pure enantiomer of histidine. The effect of the temperature and the supersaturation ratio on the nucleation rate is presented. Classic nucleation theory does not describe the data correctly and this is likely due to heterogeneous instead of homogeneous nucleation as concluded before.³⁴ It is observed experimentally that the nucleation of DL-histidine is much slower than that of L-histidine for the same level of supersaturation and at the same temperature. This has not led to preferential crystallisation of the conglomerate due to the large differences in solubility between the conglomerate and the stable racemic compound. For the racemic compound, although the crystal structure is globally compatible with the $P2_1/c$ space group, non-centrosymmetric domains are observed by SHG microscopy. As a partial reason, why CNT does not apply, the SHG signal implies that nucleation processes can in certain cases be highly complex phenomena in which the initially nucleating form loses out to the faster growing form that appears through secondary nucleation and growth, which possibly occurs on the nuclei of the initially nucleating form. Harnessing such phenomena may lead to better optimization of preferential crystallisation and separation of enantiomers by preferential enrichment.

List of symbols and abbreviations

N_A	Avogadro's constant
k	Boltzmann constant
D	Diffusion coefficient
ΔG^*	Gibbs free energy
t_g	Growth time
t_i	Induction time
C_0	Initial concentration
γ	Interfacial energy
A	Kinetic parameter
v_0	Molecular volume
J	Nucleation rate
n^*	Number of molecules in the nucleus
$P(t)$	Probability distribution
L	Pure enantiomer
DL	Racemic compound
SHG	Second harmonic generation
s	Solubility ratio
V	Solution volume
β	Supersaturation
B	Thermodynamic parameter
THG	Third harmonic generation
PXRD Powder	X-ray diffraction

Author contributions

All authors contributed equally.

Conflicts of interest

There are no conflicts to declare.

Acknowledgements

This research received funding as part of the NACRE Project by the European Regional Development Fund (FEDER) and the Normandy region. The authors thank Jules Kachaner for help with the experimental work during his internship at the SMS laboratory.

References

- 1 J. Chen, B. Sarma, J. M. B. Evans and A. S. Myerson, *Cryst. Growth Des.*, 2011, **11**, 887–895.
- 2 P. A. Larsen, D. B. Patience and J. B. Rawlings, *IEEE Control Syst.*, 2006, **26**, 70–80.
- 3 A. B. N. Brito and M. Giuliatti, *Cryst. Res. Technol.*, 2007, **42**, 583–588.
- 4 S. Suzuki and J. Mizuguchi, *Dyes Pigm.*, 2004, **61**, 69–77.
- 5 P. Muhammed Shafi and A. Chandra Bose, *AIP Adv.*, 2015, **5**, 057137.
- 6 H.-H. Tung, E. L. Paul, M. Midler and J. A. McCauley, *Crystallization of Organic Compounds: An Industrial Perspective*, John Wileys & Sons, 2009.
- 7 P. G. Vekilov, *Cryst. Growth Des.*, 2010, **10**, 5007–5019.
- 8 P. G. Vekilov, *Nat. Mater.*, 2012, **11**, 838–840.



- 9 R. P. Sear, *J. Phys. Chem. B*, 2006, **110**, 4985–4989.
- 10 X. Y. Liu, *J. Chem. Phys.*, 2000, **112**, 9949–9955.
- 11 A. Myerson, *Handbook of Industrial Crystallization*, Butterworth-Heinemann, USA, 2002.
- 12 A. Robin, P. Iavicoli, K. Wurst, M. S. Dyer, S. Haq, D. B. Amabilino and R. Raval, *Cryst. Growth Des.*, 2010, **10**, 4516–4525.
- 13 S. A. Kulkarni, S. S. Kadam, H. Meekes, A. I. Stankiewicz and J. H. Ter Horst, *Cryst. Growth Des.*, 2013, **13**, 2435–2440.
- 14 S. Jiang and J. H. Ter Horst, *Cryst. Growth Des.*, 2011, **11**, 256–261.
- 15 M. Vollmer, *Kinetik der Phasenbildung*, Verlag Theodor Steinkopff, Dresden, 1939.
- 16 A. E. Nielsen, *Kinetics of Precepitation*, Pergamon Press, Oxford, 1964.
- 17 C. Brandel and J. H. ter Horst, *Faraday Discuss.*, 2015, **179**, 199–214.
- 18 J. W. Mullin, *Crystallization*, Butterworth, London, 4th edn, 2001.
- 19 S. K. Kurtz and T. T. Perry, *J. Appl. Phys.*, 1968, **39**, 3798–3813.
- 20 D. Kashchiev and G. M. van Rosmalen, *Cryst. Res. Technol.*, 2003, **38**, 555–574.
- 21 D. Kashchiev, *Nucleation: Basic Theory With Applications*, Butterworth-Heinemann, Oxford, first, 2000.
- 22 M. P. Anisimov, *Usp. Khim.*, 2003, **72**, 664–706.
- 23 J. T. Edward, *J. Chem. Educ.*, 1970, **47**, 261–270.
- 24 M. Laliberte, *J. Chem. Eng. Data*, 2007, **52**, 1507–1508.
- 25 C. Lindenberg and M. Mazzotti, *J. Cryst. Growth*, 2009, **311**, 1178–1184.
- 26 M. Kitamura, *J. Chem. Eng. Jpn.*, 1993, **26**, 303–307.
- 27 R. J. Davey, S. L. M. Schroeder and J. H. Ter Horst, *Angew. Chem., Int. Ed.*, 2013, **52**, 2166–2179.
- 28 L. T. Padro and A. Nenes, *Atmos. Chem. Phys. Discuss.*, 2007, **7**, 2325–2355.
- 29 L. D. Shiao and H. P. Wang, *J. Cryst. Growth*, 2016, **442**, 47–51.
- 30 G. Coquerel, *J. Pharm. Pharmacol.*, 2015, **67**, 869–878.
- 31 S. Iwama, *PhD thesis*, University of Tokyo, March 2012, (thesis in Japanese).
- 32 H. Takahashi, Y. Numao, J. Motokawa, S. Clevers, G. Coquerel, H. Tsue and R. Tamura, *Chem. - Eur. J.*, 2019, **25**, 16405–16413.
- 33 G. Coquerel and M. Hoquante, *Symmetry*, 2020, **12**, 1796.
- 34 D. Gebauer, P. Raiteri, J. D. Gale and H. Cölfen, *Am. J. Sci.*, 2018, **318**, 969–988.

